

The spin-switch scanning tunneling microscopy: an architecture to probe electron-phonon interactions in the atomic scale

Dezhi Song¹, Fuyang Huang¹, Yu Gao¹, Jiamin Yao¹, Haimin Zhang¹, Haiming Huang¹, Jun Zhang^{1,*}, Xu-Cun Ma^{2,3}, Qi-Kun Xue^{2,3,4,5}, Ye-Ping Jiang^{1,†}

1 Key Laboratory of Polar Materials and Devices, Department of Electronic, East China Normal University, Shanghai, China.

2 State Key Laboratory of Low-Dimensional Quantum Physics, Department of Physics, Tsinghua University, Beijing, China.

3 Frontier Science Center for Quantum Information, Beijing, China.

4 Southern University of Science and Technology, Shenzhen, China.

5 Quantum Science Center of Guangdong-HongKong-Macao Greater Bay Area, Shenzhen, China.

On the spin-valve-like ferromagnet/spin glass/ferromagnet (FM/SG/FM) structure, the tunneling current is dominated by resistance switch (RS) instead of the local density of states according to the conventional tunneling theory. Here we show lattice-site dependent RS behaviors in one-quintuple-layer Bi_2Te_3 deposited on single MnBi_2Te_4 septuple layer, which comes from the difference in the efficiency of tunneling electrons to induce focused current or phonons at different sites, switching remotely the spin valve by spin-transfer torque or spin-phonon interactions. These lead to the observation of the dynamic 2-state lattice when the tip scans across the surface as well as the ability of scanning tunneling microscope (STM) to reveal atomic-scale features of electron-phonon (EP) interactions. Our work demonstrates the possibility of the spin-switch STM to image lattice-site dependent EP interactions of any materials deposited on the FM/SG/FM structure.

*Contact author: zhangjun@ee.ecnu.edu.cn

†Contact author: yppjiang@clpm.ecnu.edu.cn

The interactions among different degrees of freedoms in solids, such as electron-phonon (EP), spin-phonon (SP), and electron-spin (ES) interaction, etc., play key roles in a variety of disciplines. These microscopic processes are crucial for materials' properties, especially the superconductivity that involves the interactions between electrons and various kinds of bosonic excitations (1-6).

In scanning tunneling microscopy (STM), the tunneling current normally is related to the local density of states (LDOS) and the images taken with a constant current show spatial variation of LDOS at the surface (7). One of the most important variations of STM utilize the inelastic processes induced by the hot electrons from the tip (8, 9), including the ES interactions that generate spin-flip excitations or EP interactions that generate phonons. These kinds of inelastic electron tunneling spectroscopy (IETS) yield the ability of STM to detect spin states (10-17) or phonon modes (18-21) at the atomic scale. Yet most of previous IETS methods only work on single adatoms, molecules or nano-sized structures on top of the surface (22, 23), where the elemental excitations in these structures provide additional tunneling channels in the tip-substrate junction and show as IETS features in the spectra. It is because normally IETS due to phonon or other bosonic modes doesn't have enough contrast between different lattice positions in a flat film, except for some special cases of metal surfaces (24) or the case with combined effect from EP interactions and electron interference (18).

In this report, we demonstrate a kind of spin-switch (SS)-STM that can be used to detect EP interactions in thin films with atomic resolution. The key ingredient in our method is a spin-valve-like ferromagnet/spin glass/ferromagnet (FM/SG/FM) layer, on top of which the film of interest can be deposited. As demonstrated by our previous work (25), the spin states of the spin-valve layer can be switched remotely and show as the resistance-switch (RS) between $\downarrow \rightarrow \downarrow$ (state 1) and $\downarrow \uparrow \downarrow$ (state 2) configurations by the tunneling current in the EP/SP- or the spin-transfer-torque (STT)-dominated situations, respectively. Here we show that these two competing switch trends between EP/SP and STT behave differently at different lattice-sites on the surface. This comes from the difference in the efficiency of tunneling electrons at different positions to stimulate phonons and focused current to switch the SG-layer spins. This behavior exists even in the presence of additional overlayers of another material. Note that the tunneling current is dominated by RS of the spin-valve layer. These lead to the observation of the dynamic 2-state lattice superimposed on the original lattice of the overlayer when the tip scans across the surface at

*Contact author: zhangjun@ee.ecnu.edu.cn

†Contact author: ypjiaang@clpm.ecnu.edu.cn

appropriate working currents and electron energies, switching the local spin alignments toward $\downarrow \rightarrow \downarrow$ and $\downarrow \uparrow \downarrow$ alternatively at different lattice sites. Furthermore, the SS-STM is able to image sub-surface lattice features and even features between lattice-positions of the overlayer resulted from different EP interactions at different positions.

The double tunneling junction in SS-STM

In our architecture of SS-STM, the one septuple layer (SL) of MnBi_2Te_4 (MBT) constitutes the spin-valve layer. As shown in the schematic in Fig. 1 (left), in the presence of dilute Mn-doping in the Bi-layers, the 1-SL MBT has a ferrimagnetic (FiM) ground state between the Mn-layer and Bi-layer spins (26). The Mn-layer spins can be doped by Bi into a SG-like state with a reduced FM transition temperature T_{c1} . The SS-STM works above T_{c1} of the SG layer and below T_{c2} of the dilute Mn-doped Bi-layers, where the spin states then become highly switchable by SP/STT in the limit of single spin as shown in Fig. 1 (right). The 1-SL MBT is slightly *n*-doped so that the charge current across the MBT is conducted by hopping along the $pp\sigma$ chains of *p*-orbitals of Bi and Te (27), which are much reduced in the Mn-layer. This constitutes the second tunneling junction, the resistance of which is dominated by RS due to different spin alignments. The double-junction structure preserves in the presence of a Bi_2Te_3 (BT) overlayer.

The tip used here is non-magnetic instead of spin-polarized (28), providing incident hot electrons with precise energies. Above the exchange energy E_{ex} (between itinerate electrons and Mn-layer spins) the spin-flip interactions drive the spin-valve layer toward the parallel $\downarrow \downarrow \downarrow$ alignment. Below E_{ex} , phonons stimulated by hot tunneling electrons thermalize the SG-layer by SP interactions while the current polarize the SG-layer spins by STT (26), switching the local magnetic alignment toward with low (state 1, $\downarrow \rightarrow \downarrow$) and high resistances ($\downarrow \uparrow \downarrow$, state 2), respectively. In the presence of strong EP interactions, the incident tunneling current becomes less focused because of scattering, reducing STT and leading to the phonon-dominated situation.

The current-dependent RS on the BT overlayer

In the dI/dV spectra taken on the spin-valve layer, the tunneling conductance σ corresponds to the LDOS as usual at $E > E_{\text{ex}}$. At $E \leq E_{\text{ex}}$, σ is dominated by RS, where SP competes with STT. The SP- and STT-dominated states are denoted as states 1 and 2 (Fig. 2(A)), respectively. In state 1, the spectrum shows enhanced conductance below E_{ph} , which indicates the phonon-dominated energy region. E_{ph} usually is related to the energy limit E_{pl} (~ 17 meV) of phonons in MBT. As for

*Contact author: zhangjun@ee.ecnu.edu.cn

†Contact author: ypjiaang@clpm.ecnu.edu.cn

E_{ex} , we observe two conditions with $E_{ex} \sim 17$ meV and $E_{ex} \sim 40$ meV, where the former may abruptly switch into the latter due to possible switch between metastable magnetism in the SG-layer.

Similar to those on MBT (26), the RS behaviors on the BT overlayer evolve from state 1 to state 2 with I_g (the tunneling current at the bias voltage of 100 mV), which means that STT dominates over SP at higher tunneling currents. As shown in Figs. 2(B) and 2(C), the dI/dV and $I-V$ spectra taken on the surface Te positions (Te1 in Fig. 1(A)) show enhanced or reduced conductance at lower or higher I_g below E_{ex} (~ 17 meV). The spectra taken on the off-Te1 positions show similar behaviors (Figs. 2(C) and 2(D)).

The site-dependent RS and the dynamic 2-state lattice

By plotting the I_g -dependent RS spectra on these two lattice positions into colored figures in Fig. 3(A), the site-dependence of RS becomes evident. In contrast to those taken on Te1, there is a noticeable state 2 region at low I_g in the off-Te1 RS. As a result, the state 1 region (indicated by dashed lines in Fig. 3(A)) of off-Te1 RS is much narrower than that of on-Te1 RS. Hence, as indicated by triangles in Fig. 3(A) and the corresponding RS spectra in Fig. 3(B), the RS can be at states 1 or 2 at the same lattice site depending on I_g or at the same I_g depending on lattice sites.

We take the STM images in the constant current mode on the BT overlayer below E_{ex} with different tunneling currents. In this mode, the metallic tip's height normally changes in accord with the constant contour of the function $\int_0^{eV_{Bias}} LDOS(E, \mathbf{r}) dE$ according to conventional scanning tunneling theory. Here with a spin-valve underlayer, the STM images on the BT overlayer show peculiar behaviors as shown in Fig. 3(C). Figure 3(C)-(i) taken at 1 eV shows the normal morphology of the BT surface, where the darker triangular features are the Mn-on-Bi1 (Mn_{Bi1}) anti-site defects. The STM images taken at 10 meV in Figs. 3(C)-(ii-iv) shows that the film is in the state 1, state 2, and mixed state at tunneling current 5 pA, 50 pA and 15 pA, respectively. Note that I_g are about 100 pA and 2 nA for the tunneling currents of 5 pA and 50 pA at 10 meV. In Fig. 3(C)-(iii), the mixed condition indicates that the switch currents between state 1 and state 2 is not uniform across the sample. The 'height' difference between the state-1 and state-2 regions is about 0.1 nm, which means that the tip needs to approach the sample surface by 0.1 nm to keep the constant tunneling current of 15 pA in the region where the spin-valve layer is in the high resistive state 2. Hence, the STM image, which we then call the RS image, no longer

*Contact author: zhangjun@ee.ecnu.edu.cn

† Contact author: yppjiang@clpm.ecnu.edu.cn

corresponds to the surface morphology or LDOS features. A closer inspection in Fig. 3(D) shows that the RS images show depressions at the Bi1 sites or at the Te1 sites when being in state 1 or state 2, respectively. This correspondence is obtained by taking the dI/dV mapping near the Mn_{Bi1} defect, which takes the defect position and the RS images simultaneously (Extended data Fig. 9).

These lead to the realization of a dynamic 2-state lattice at certain current (11 pA), which is just below the critical current of the region to switch from state 1 to state 2. Because of the site-dependent RS behaviors, the critical currents at different lattice positions are slightly different. As shown in Fig. 3(E), the Bi1 sites and the regions around the Mn_{Bi1} defects (circled region) enters state 2 first and show huge depressions of about 0.1 nm in depth (inserted line profile). In contrast, the three nearest Te1 sites around the Mn_{Bi1} defect keep at state 1 until the whole region turns into state 2. This indicates the ability of SS-STM to detect atomic-scale variations of EP interactions due to the presence of single defects.

Hence, at an appropriate tunneling current, the spin-valve layer switches locally between states 1 and 2 (insert) when scanning the tip across the surface of BT overlayer below E_{ex} , forming a lattice with alternating conductance as illustrated in Fig. 3(F) (bottom), where the top one shows the top-view of the lattice structure of BT. The dashed line indicates the Bi1 line along which the line profile in Fig. 3(E) is taken.

Imaging the sub-surface features of EP interactions

Since the tunneling no longer depends on the LDOS features near the surface but on the ability of the tunneling electrons to stimulate specific phonon modes or focused current to switch remotely the spin alignment in the spin-valve layer, the RS images now can give information of EP interactions in the BT overlayer. Figures 4(A) and 4(B) are the images taken on BT with the spin-valve layer being at state 1 and state 2, respectively. The image taken at state 1 show depressed features at all the surface and sub-surface lattice positions (Te1/Bi2, Bi1/Te3, Te2) projected onto the surface. A lower height in the RS image means a higher resistance. This implies a more focused current or less created phonons when tunneling directly onto atoms. We also notice the one-dimensional features along Te2 which at this stage we have no explanations. The RS image taken at state 2 (Fig. 4(B)) shows much different features. There is a large depressed region near the Te1/Bi2 position. Nonetheless, compared with the case at state 1, all the lattice positions also show features with reduced conductance.

*Contact author: zhangjun@ee.ecnu.edu.cn

†Contact author: yppiang@clpm.ecnu.edu.cn

When the spin-valve underlayer is in a different magnetic state ($E_{\text{ex}} \sim 40$ meV, Fig. S6 of (29)), the RS images taken on the BT overlayer show a much complicated pattern. Compared to the dark spots on lattice positions in Fig. 4(A), the spot-like features as shown in Fig. 4(C) are on off-site positions and are bright (correspond to enhanced conductance), especially the dash-circled one. The lattice positions still have reduced conductance. This may be due to the enhanced probabilities of incident tunneling electrons to stimulate specific phonon modes on some atomic bonds that can more easily propagate into the spin-valve layer and thermalize the SG-layer spins by SP interactions.

Discussion and conclusion

Our observation in the BT/MBT system might be generalizable and applied to other systems. Considering, for instance, some kind of material having a lattice with the form $\mathbf{r}_{ij} = \mathbf{R}_i + \mathbf{r}_j$, is deposited on some spin-valve layer. Here $\mathbf{R}_i, \mathbf{r}_j$ are the translational vectors and the atomic positions in one unit cell, respectively. We assume an infinite small radius of tunneling region, so that the probability of creating specific phonon mode at position \mathbf{r} is $p_k(\mathbf{r})$ instead of some weighted integral. Then the remaining focused current $I = I_0(1 - \sum_k p_k(\mathbf{r}))$, where the sum is over all the phonon modes. Here I_0 is the tunneling current from the tip at some energy below E_{ex} . The resulting tunneling conductance that depends on the spin-valve layer is then some function of the focused current and the stimulated phonon modes in the overlayer $\sigma = f(I, \{p_k(\mathbf{r})\})$. Indeed, if the phonon modes between the overlayer and the spin-valve layer don't match well in contrast to the present BT/MBT case so that the phonon-phonon interactions across the interface is weak, $\sigma \approx f(I) = f(I_0(1 - \sum_k p_k(\mathbf{r})))$ is still some function of $p_k(\mathbf{r})$. Thus, the SS-STM image that corresponds to the conductance map $\sigma(\mathbf{r})$ reflects the map of EP interactions at each specific position at any energies below E_{ex} of hot electrons. From this point of view, Fig. 4(C) tells that the largest probability of EP scattering as well as creating specific phonon modes that disturb the spin-valve layer most is at some atomic bonds instead of lattice positions.

The ability of the spin-switch STM might be further generalized to the investigation of the interactions between electrons and any other elemental excitations in solids, especially near some crystal defects. Our proposed SS-STM provides an atomic-scale method to investigate the interactions between these important degrees of freedoms in an architecture that can be possibly applied to other systems.

*Contact author: zhangjun@ee.ecnu.edu.cn

†Contact author: ypjia@clpm.ecnu.edu.cn

References

1. J. P. Carbotte, T. Timusk, J. Hwang, Bosons in high-temperature superconductors: an experimental survey. *Rep. Prog. Phys.* **74**, 066501 (2011).
2. J. Lee *et al.*, Interplay of electron–lattice interactions and superconductivity in $\text{Bi}_2\text{Sr}_2\text{CaCu}_2\text{O}_{8+\delta}$. *Nature* **442**, 546-550 (2006).
3. L. Wang, X. Ma, Q.-K. Xue, Interface high-temperature superconductivity. *Supercond. Sci. Technol.* **29**, 123001 (2016).
4. V. Z. Kresin, S. A. Wolf, Colloquium: Electron-lattice interaction and its impact on high T_c superconductivity. *Rev. Mod. Phys.* **81**, 481-501 (2009).
5. S. Dal Conte *et al.*, Disentangling the Electronic and Phononic Glue in a High- T_c Superconductor. *Science* **335**, 1600-1603 (2012).
6. J. Bardeen, L. N. Cooper, J. R. Schrieffer, Theory of Superconductivity. *Physical Review* **108**, 1175-1204 (1957).
7. J. Tersoff, D. R. Hamann, Theory of the scanning tunneling microscope. *Phys. Rev. B* **31**, 805-813 (1985).
8. T. Komeda, N. Okabayashi, in *Springer Handbook of Surface Science*, M. Rocca, T. S. Rahman, L. Vattuone, Eds. (Springer International Publishing, Cham, 2020), pp. 815-852.
9. S. You, J.-T. Lü, J. Guo, Y. Jiang, Recent advances in inelastic electron tunneling spectroscopy. *Adv. Phys.: X* **2**, 907-936 (2017).
10. J. Fernández-Rossier, Theory of Single-Spin Inelastic Tunneling Spectroscopy. *Phys. Rev. Lett.* **102**, 256802 (2009).
11. S. Rolf-Pissarczyk *et al.*, Dynamical Negative Differential Resistance in Antiferromagnetically Coupled Few-Atom Spin Chains. *Phys. Rev. Lett.* **119**, 217201 (2017).
12. S. Baumann *et al.*, Electron paramagnetic resonance of individual atoms on a surface. *Science* **350**, 417-420 (2015).
13. F. Donati *et al.*, Magnetic remanence in single atoms. *Science* **352**, 318-321 (2016).
14. A. J. Heinrich, J. A. Gupta, C. P. Lutz, D. M. Eigler, Single-Atom Spin-Flip Spectroscopy. *Science* **306**, 466-469 (2004).
15. S. Loth, M. Etzkorn, C. P. Lutz, D. M. Eigler, A. J. Heinrich, Measurement of Fast Electron Spin Relaxation Times with Atomic Resolution. *Science* **329**, 1628-1630 (2010).
16. Y. Wang *et al.*, An atomic-scale multi-qubit platform. *Science* **382**, 87-92 (2023).
17. K. Yang *et al.*, Coherent spin manipulation of individual atoms on a surface. *Science* **366**, 509-512 (2019).
18. I. Altfeder, K. A. Matveev, A. A. Voevodin, Imaging the Electron-Phonon Interaction at the Atomic Scale. *Phys. Rev. Lett.* **109**, 166402 (2012).
19. M. Grobis *et al.*, Spatially Dependent Inelastic Tunneling in a Single Metallofullerene. *Phys. Rev. Lett.* **94**, 136802 (2005).
20. B. C. Stipe, M. A. Rezaei, W. Ho, Inducing and Viewing the Rotational Motion of a Single Molecule. *Science* **279**, 1907-1909 (1998).
21. L. J. Lauhon, W. Ho, Electronic and vibrational excitation of single molecules with a scanning tunneling microscope. *Surf. Sci.* **451**, 219-225 (2000).

*Contact author: zhangjun@ee.ecnu.edu.cn

†Contact author: ypijiang@clpm.ecnu.edu.cn

22. D.-J. Choi *et al.*, Colloquium: Atomic spin chains on surfaces. *Rev. Mod. Phys.* **91**, 041001 (2019).
23. S. Loth, S. Baumann, C. P. Lutz, D. M. Eigler, A. J. Heinrich, Bistability in Atomic-Scale Antiferromagnets. *Science* **335**, 196-199 (2012).
24. H. Gawronski, M. Mehlhorn, K. Morgenstern, Imaging Phonon Excitation with Atomic Resolution. *Science* **319**, 930-933 (2008).
25. D. Song *et al.*, Resistance switch in ferromagnet/spin glass/ferromagnet spin valves. *arXiv:2412.05960*, (2024).
26. D. Song *et al.*, The re-entrant ferromagnetism due to symmetric exchange bias in two septuple-layer MnBi₂Te₄ epitaxial films. *arXiv:2412.05959*, (2024).
27. Y. Jiang *et al.*, Fermi-Level Tuning of Epitaxial Sb₂Te₃ Thin Films on Graphene by Regulating Intrinsic Defects and Substrate Transfer Doping. *Phys. Rev. Lett.* **108**, 066809 (2012).
28. R. Wiesendanger, Spin mapping at the nanoscale and atomic scale. *Rev. Mod. Phys.* **81**, 1495-1550 (2009).
29. See the supplementray materials.

*Contact author: zhangjun@ee.ecnu.edu.cn

†Contact author: ypjiaang@clpm.ecnu.edu.cn

Figure captions

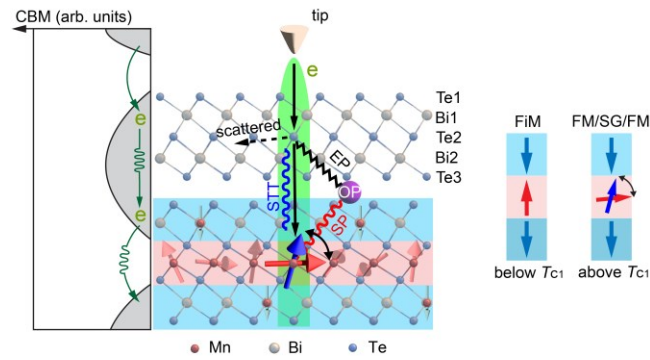


Fig. 1. Schematic of FM/SG/FM spin valves and RS mechanisms in BT/MBT. The double-barrier junction and the microscopic processes in BT/MBT responsible for the RS behaviors. The 1-SL MBT is FiM below T_{c1} . The RS appears above T_{c1} where the Mn-layer spins are SG-like and become highly switchable by tunneling electrons.

*Contact author: zhangjun@ee.ecnu.edu.cn

†Contact author: ypjiaang@clpm.ecnu.edu.cn

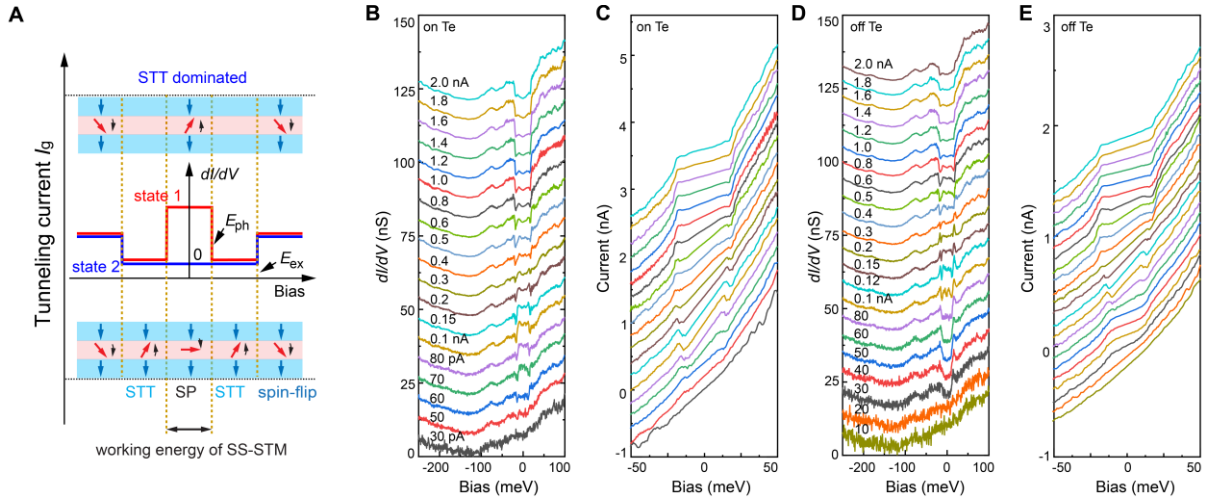


Fig. 2. The current-dependence of RS behaviors in BT/MBT. (A) The correspondence between different conductance states in the dI/dV curves and the underlying switching processes. **(B)-(D)** The current-dependent dI/dV and $I-V$ spectra taken at 8 K on the top-Te and on the off-Te positions, respectively. The temperature is at 8 K. The Bi_{Mn} doping x of the BT/MBT film is 0.28. At 8 K, the dilute Mn_{Bi} -doped Bi-layers are FM and the Mn-layer is in the SG state. All the spectra are normalized to $I_g = 2 \text{ nA}$.

*Contact author: zhangjun@ee.ecnu.edu.cn

†Contact author: ypjia@clpm.ecnu.edu.cn

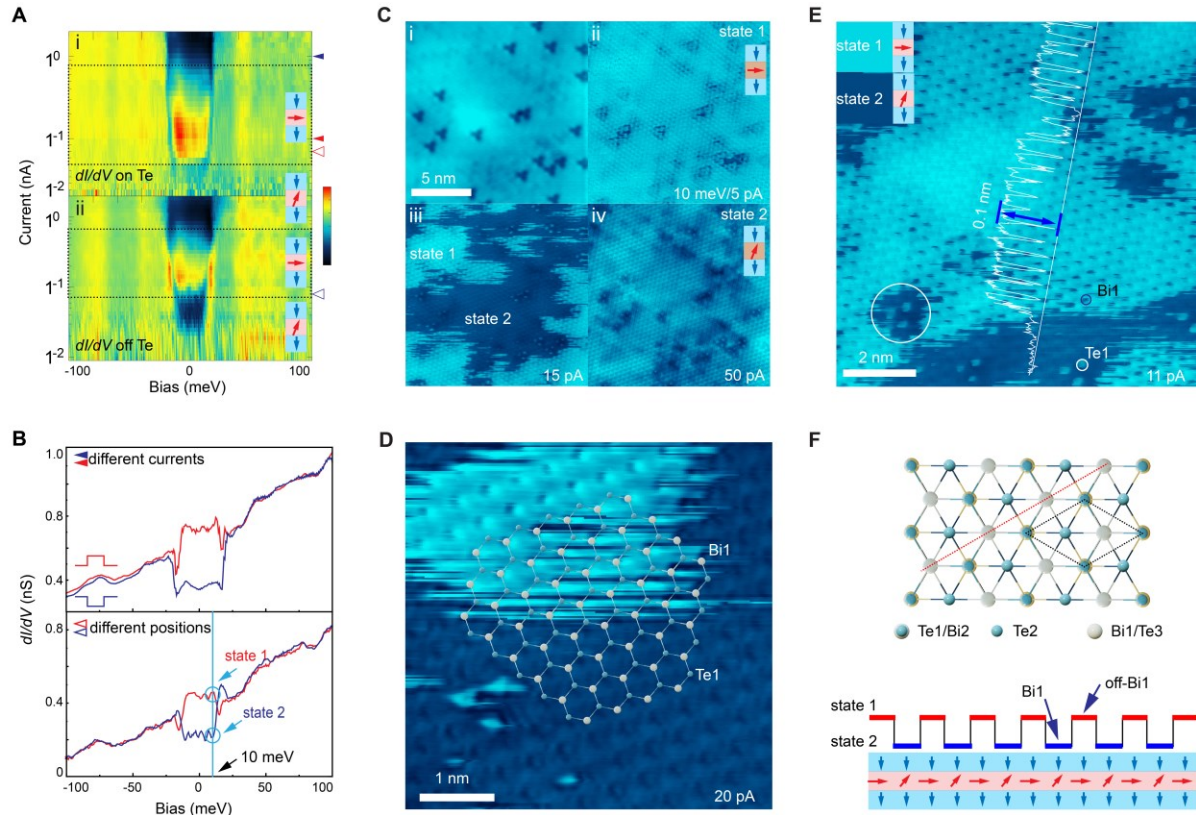


Fig. 3. The atomically resolved RS and the 2-state lattice in BT/MBT films. (A) The colored maps correspond to the current-dependent RS behaviors in Fig. 2. All the spectra are background-subtracted. **(B)** Different resistance state (1 and 2) obtained at different I_g (100 pA and 1 nA) at the same position (on Te1) as well as those obtained at the same I_g (80 pA) but at different positions (on Te1 and off Te1). The solid and hollow arrows indicate the correspondence between (A) and (B). **(C)** STM images taken at different tunneling conditions (1 V, 50 pA; 10 mV, 5 pA; 10 mV, 15 pA; 10 mV, 50 pA). **(D)** A zoom-in image in the mixed condition showing the different atomically-resolved ‘lattices’ for states 1 and 2. **(E)** The mixed state taken at (10 mV, 11 pA) showing the breaking-down of the state 1 at 1st-Bi sites. The inserted line profile shows the tip-height change in response to the alternate switching between states 1 and 2 along 1st-Bi chain (white line). **(F)** The top-view crystal structure of BT (top) and the schematic of the switch between states 1 and 2 along Bi1 line (bottom). The dashed line indicates the Bi1 line. The dashed rhombus denotes the surface unit cell.

*Contact author: zhangjun@ee.ecnu.edu.cn

† Contact author: yjjiang@clpm.ecnu.edu.cn

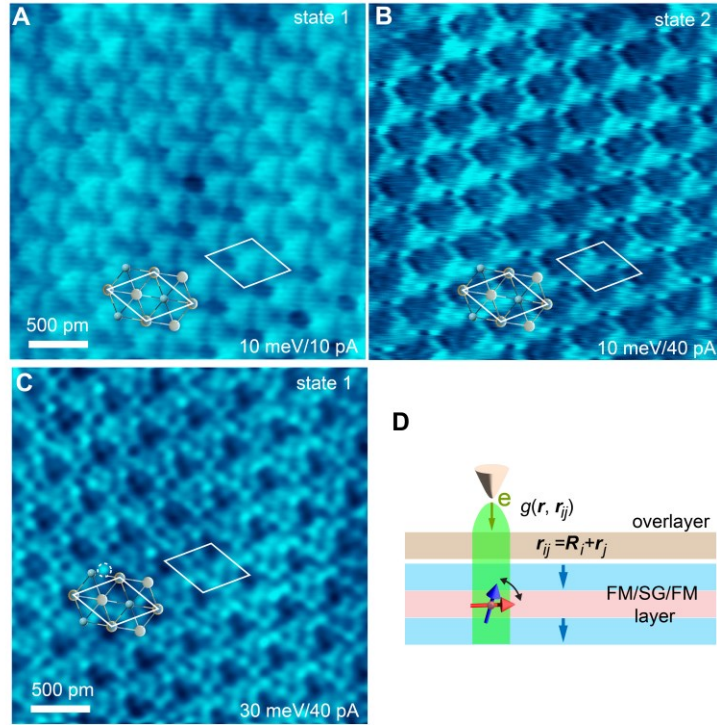


Fig. 4. The dI/dV mapping of BT/MBT/BT film. (A) (B) STM images taken at state 1 (10 mV, 10 pA) and state 2 (10 mV, 40 pA), respectively. (C) The STM image (10 mV, 10 pA) of BT taken at state 1 of MBT in a different condition. (D) The schematic of spin-switch STM.

*Contact author: zhangjun@ee.ecnu.edu.cn

† Contact author: yppiang@clpm.ecnu.edu.cn

Acknowledgments

We acknowledge the supporting from National Key R&D Program of China (Grants No. 2022YFA1403102) and National Science Foundation (Grants No. 92065102, 61804056, 12134008).

Author contributions

Y-. P. J. conceived and designed the experiments. D. S., F. H., Y. G., J. Y., H. Z., and H. H. carried out MBE growth and STM measurements. Y-. P. J. did the transport measurement. Y-. P. J. and J. Z. did data analyses and interpretations. Y-. P. J wrote the manuscript, with input from all authors.

Competing interests

The authors declare that they have no competing interests.

Data and materials availability

All data are available in the main text or the supplementary materials.

Supplementary Materials

Materials and Methods

Figs. S1 to S6

*Contact author: zhangjun@ee.ecnu.edu.cn

†Contact author: ypjia@clpm.ecnu.edu.cn



Supplementary Materials for

The spin-switch scanning tunneling microscopy: an architecture to probe electron-phonon interactions in the atomic scale

Dezhi Song¹, Fuyang Huang¹, Yu Gao¹, Jiamin Yao¹, Haimin Zhang¹, Haiming Huang¹, Jun Zhang^{1,*}, Xu-Cun Ma^{2,3}, Qi-Kun Xue^{2,3,4,5}, Ye-Ping Jiang^{1,†}

1 Key Laboratory of Polar Materials and Devices, Department of Electronic, East China Normal University, Shanghai, China.

2 State Key Laboratory of Low-Dimensional Quantum Physics, Department of Physics, Tsinghua University, Beijing, China.

3 Frontier Science Center for Quantum Information, Beijing, China.

4 Southern University of Science and Technology, Shenzhen, China.

5 Quantum Science Center of Guangdong-HongKong-Macao Greater Bay Area, Shenzhen, China.

*Corresponding author. Email: zhangjun@ee.ecnu.edu.cn, ypjiang@clpm.ecnu.edu.cn

The PDF file includes:

Materials and Methods
Figs. S1 to S6

Materials and Methods

Sample preparation

To improve the crystal quality of the 1-SL MBT (the spin-valve layer), a 1-QL BT layer was grown on the STO (111) substrate. All the heterostructures of MBT and BT were grown in a step-wise manner, that is, only one QL or SL was deposited and annealed at 250 °C each time. The quality of the film was checked by STM between successive growth steps.

STM measurement

The experiments were performed in an ultrahigh vacuum (UHV) system with a magnetic-field (up to 15 T) equipped cryogenic STM and an MBE. The temperature of the STM can be varied from 4.3 K to about 30 K to carry out the measurements of topography and spectroscopy. The STM measurements were performed using a non-magnetic W tip. The chemically-etched W tip was transferred into MBE and annealed to about 1000 °C to get rid of contaminations. The metallic tip condition was obtained and checked in STM on Ag islands grown on the silicon substrate.

STM topography measurements were performed at a constant tunneling current with an active feedback loop. During the spectroscopy measurements, dI/dV or current signals were recorded while keeping the feedback off (lock-in bias modulation: 3 mV at 987.5 Hz; bias steps: 512; sampling interval: 20 ms). All the energies are shown with respect to the Fermi level. The STM images were processed using WSxM software. The current dependent colored-maps for dI/dV and $I-V$ spectra were plotted using MATLAB. All images and spectra are raw data without any post-processing unless otherwise specified.

The two types of magnetic states of the spin-valve layer

As shown in Fig. 2 and Fig. S6, the BT/MBT film shows two kinds of RS spectra that have two different exchange energies E_{ex} . In our experiments, we find that the MBT films only show the state with the larger E_{ex} . After the deposition of the additional BT layer, the BT/MBT film was first in the state with the smaller E_{ex} and switched to the state with the larger E_{ex} in one or two days of scanning the surface. The switch is abrupt and may be due to the strain releasing between BT and MBT. The strain releasing seems to also change the magnetic state or the exchange energy. We checked the tip's condition before and after each experiment and we are sure that the tip was metallic and clean for all the data taken in our work

Supplementary figures

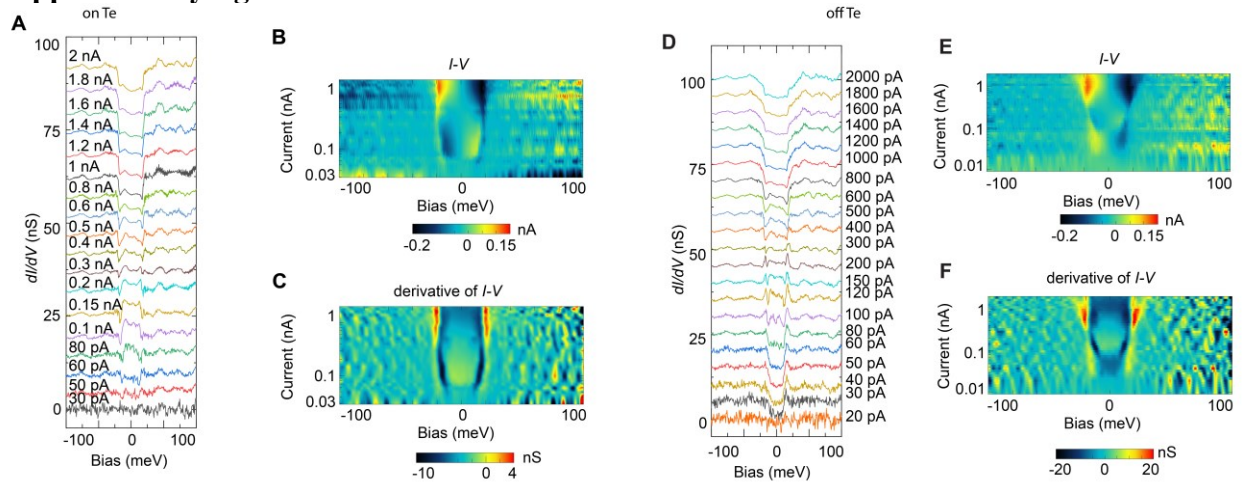


Fig. S1 The supplementary data for Fig. 2. **(A)-(C)** The background-subtracted tunneling (I_g)-dependent dI/dV spectra, the colored maps of $I-V$ and the 1st-derivative of $I-V$ spectra at the surface Te1 position. **(D)-(E)** The data on the off-Te1 position.

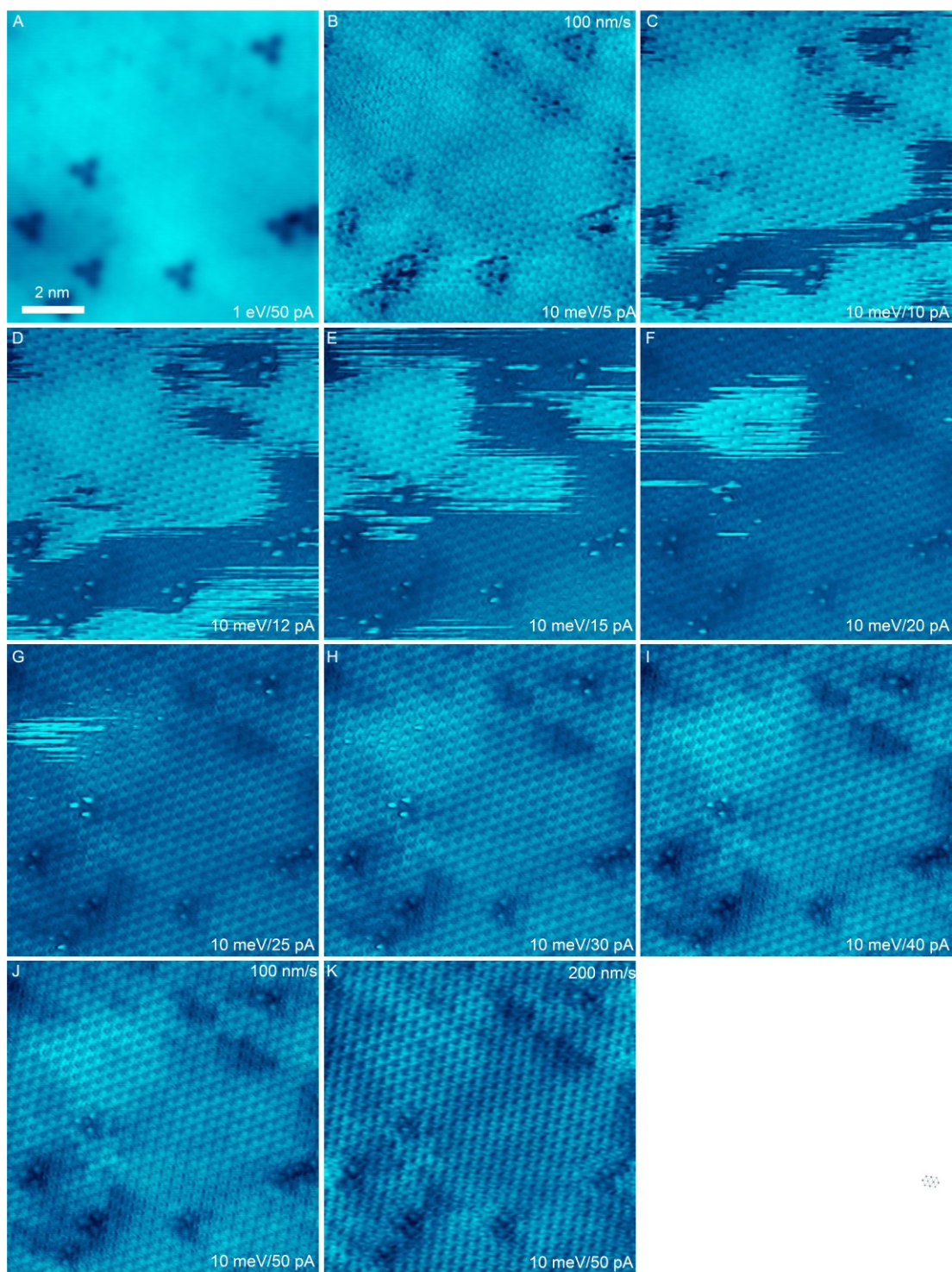


Fig. S2 The supplementary data for Fig. 3(C). (A) The STM image taken (1 V, 50 pA). (B)-(I) RS images taken at 10 meV and at different currents. The scan speed of the tip is 200 nm/s. (J)(K) The comparison between the RS images taken at the same condition but with different scanning speeds.

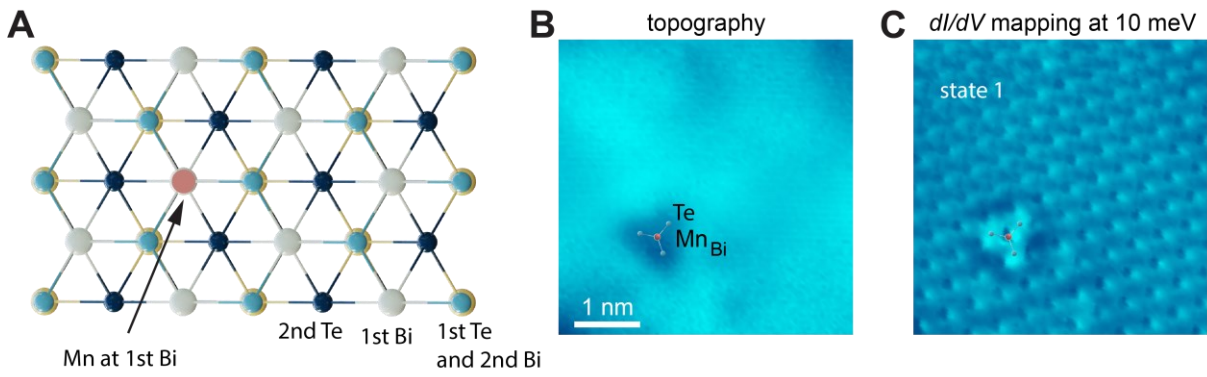


Fig. S3 The dI/dV mapping of BT/MBT/BT film in Fig. 4. (A) The top-view crystal structure of BT. The arrow indicates a Mn_{Bi} anti-site defect. (B)(C) The STM image (1 V, 50 pA) and the corresponding dI/dV mapping at 10 meV of the BT/MBT/BT surface (in state 1).

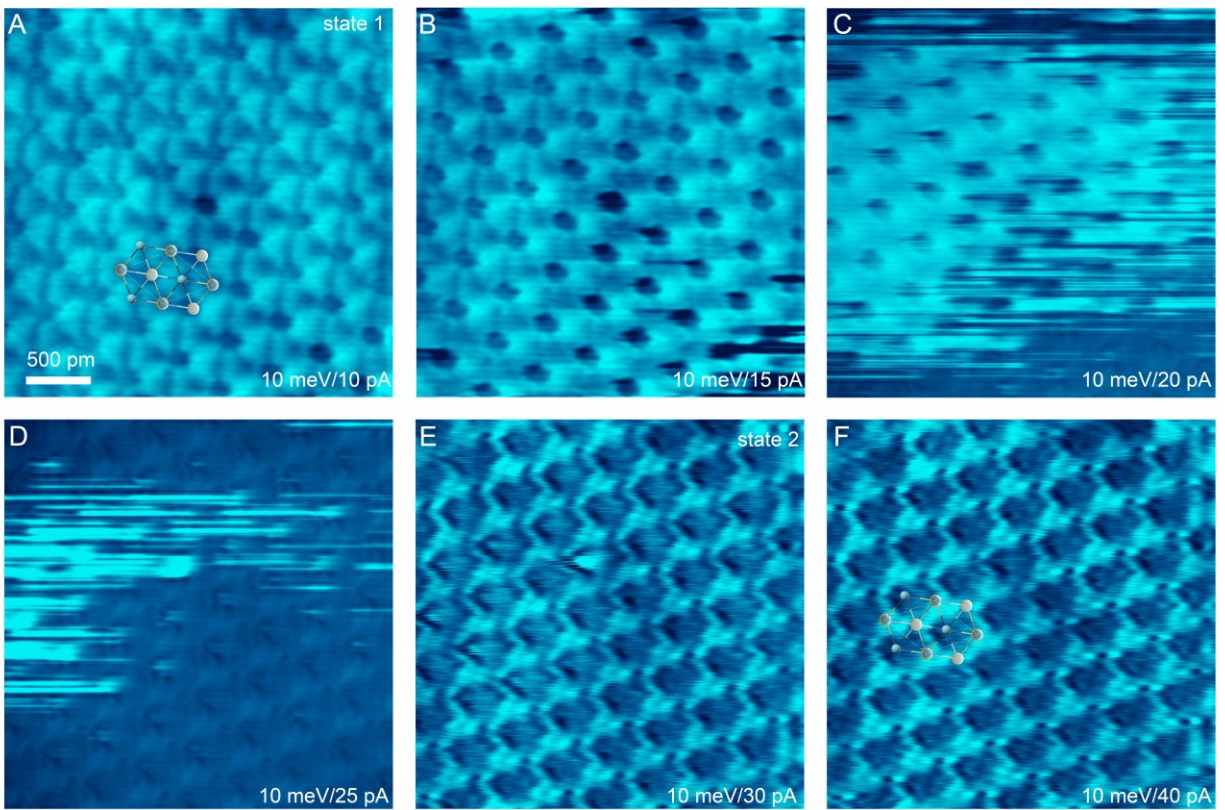


Fig. S4 The RS images supplementary to Figs. 4(A) and 4(B). These RS images are taken at 10 meV and at different currents. (A)-(B) are at state 1. (C)-(D) are at the mixed state. (E)-(F) are at state 2.

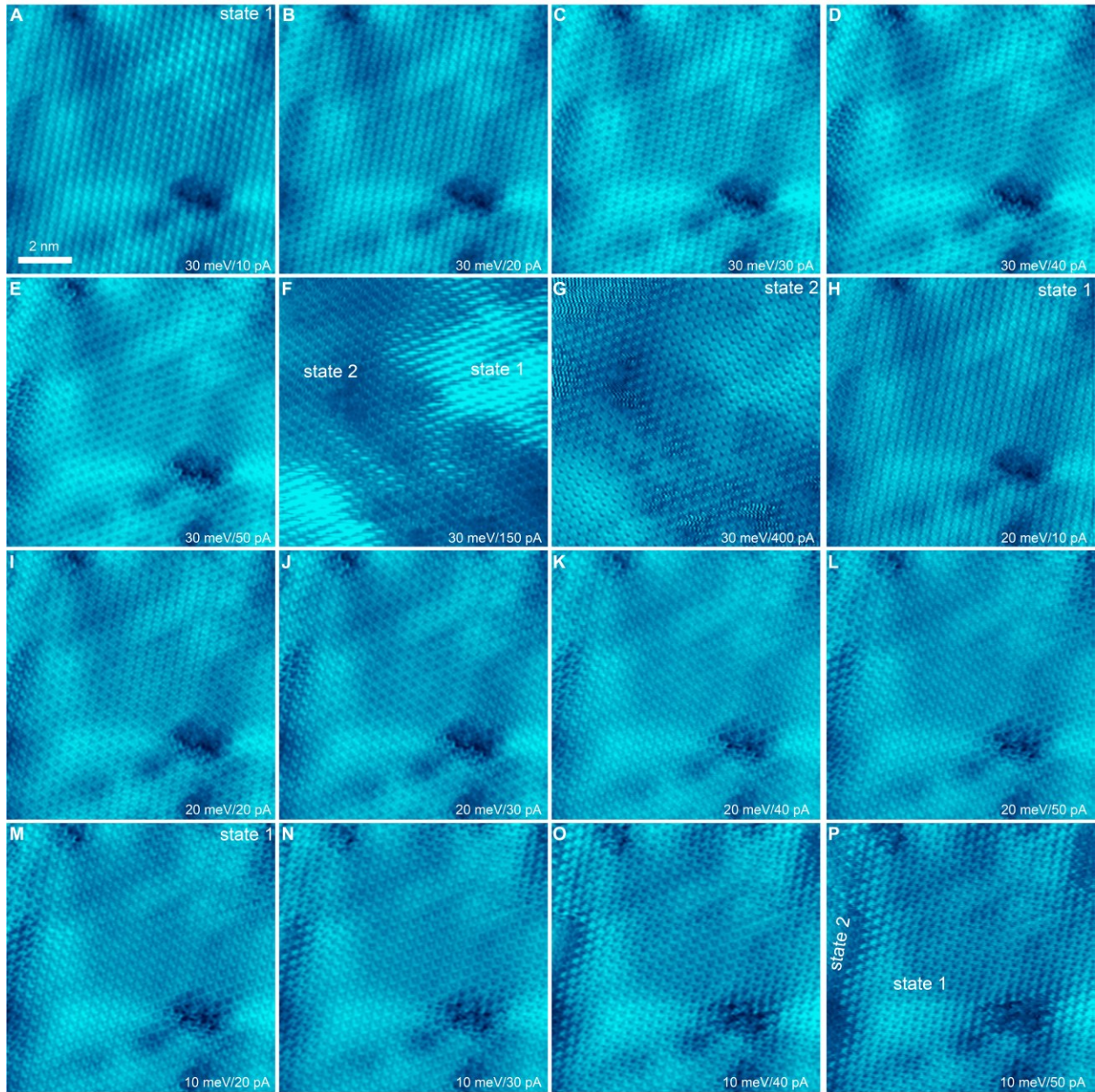


Fig. S5 The RS images supplementary to Fig. 4(C). (A)-(G) The RS images taken at 30 meV and at different currents. (A)-(E) are at state 1. (F) is at the mixed state. (G) is at state 2. (H)-(L) The RS images taken at 20 meV and at different currents. Up to 50 pA all of the RS images are at state 1. (M)-(P) The RS images taken at 10 meV and at different currents. (M) is at state 1. (N)-(P) are at the mixed state.

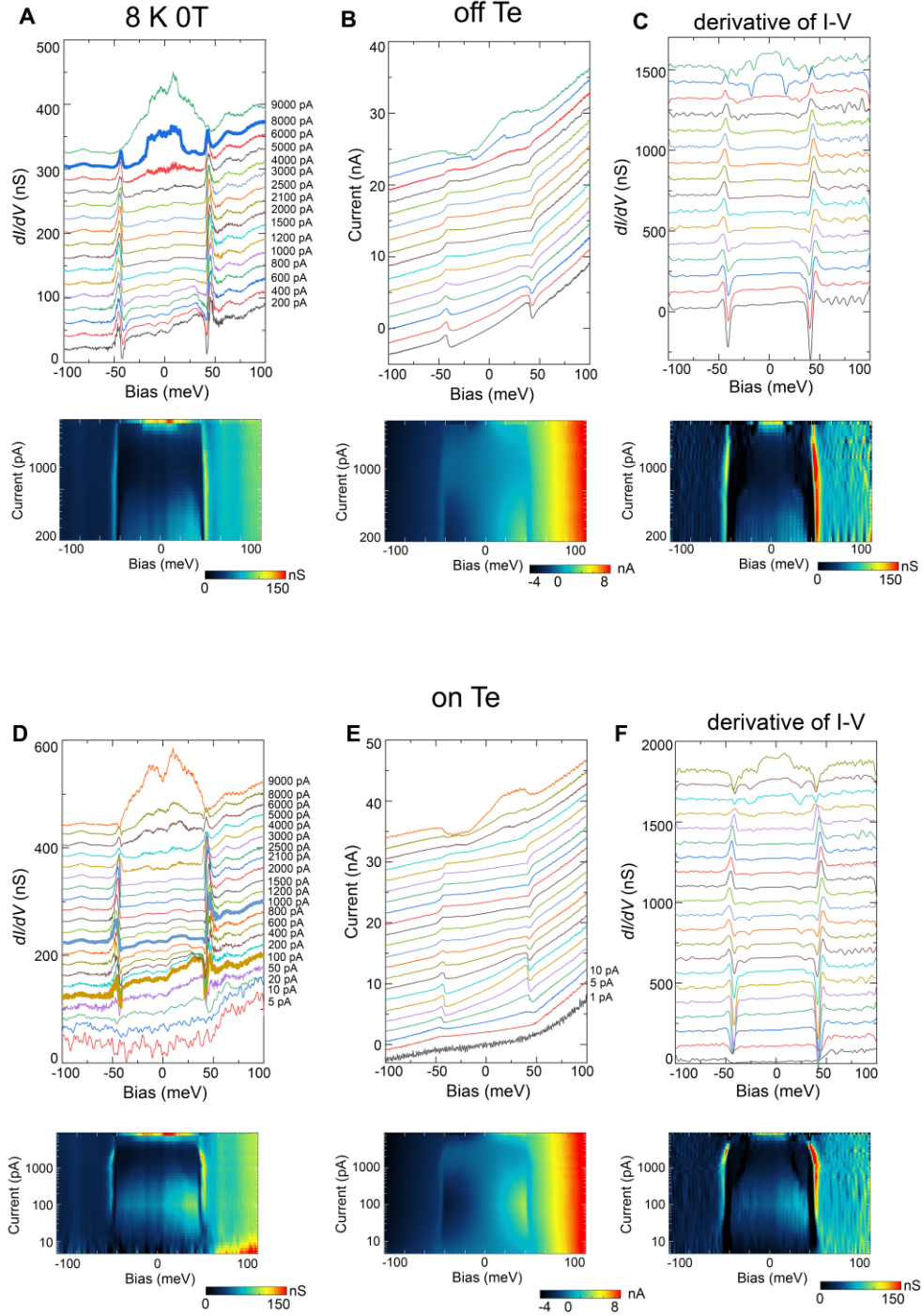


Fig. S6 The final relaxed state of the BT/MBT film in Fig. 4(C). (A)-(C) The tunneling (I_g) dependent dI/dV , I - V , 1st-derivative of I - V spectra at the surface Te positions. The bottom figures are the corresponding colored-images. (D)-(F) The data at the off-Te positions.